Sub-sample time shift and horizontal displacement measurements using phase correlation method in time-lapse seismic

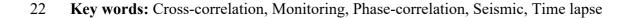
3 Gaurav Tomar<sup>1</sup>, Satish C. Singh<sup>1</sup> and Jean-Paul Montagner<sup>1</sup>

4 1. Institut de Physique du Globe de Paris, Sorbonne Paris Cité, CNRS (UMR 7154), Paris, France

## 5 Abstract

6 Hydrocarbon production and fluid injection affect the level of subsurface stress, physical 7 properties of the subsurface, and can cause reservoir-related issues, such as compaction and 8 subsidence. Monitoring of oil and gas reservoirs is therefore crucial. Time-lapse seismic is 9 used to monitor reservoirs and provide evidence of saturation and pressure changes within the 10 reservoir. However, relative to background velocities and reflector depths, the time-lapse 11 changes in velocity and geomechanical properties are typically small between consecutive 12 surveys. These changes can be measured by using apparent displacement between migrated 13 images obtained from recorded data of multiple time-lapse surveys. Apparent displacement 14 measurements by using the classical cross-correlation method are poorly resolved. Here, we 15 propose the use of a phase-correlation method, which has been developed in satellite imaging 16 for sub-pixel registration of the images, to overcome the limitations of cross-correlation. 17 Phase-correlation provides both vertical and horizontal displacements with a much better 18 resolution. After testing the method on synthetic data, we apply it to a real data set from the 19 Norne oil field and show that the phase correlation method can indeed provide better 20 resolution.

21



#### 1 1. Introduction

2 Time-lapse seismic has proven to be a useful tool for reservoir monitoring. It is increasingly 3 becoming a standard method to identify undrained resources, to monitor hydrocarbon 4 production and costly injected fluids like gas, water and carbon dioxide (CO<sub>2</sub>) (Landro 1999, 5 Johnston 2013). Hydrocarbon production and fluid injection affect the level of subsurface 6 stress and physical properties of the subsurface during the life of an oil or gas field and can 7 cause some production challenges, such as compaction and subsidence. In the subsurface, 8 these geomechanical changes can be measured by using apparent displacement between 9 migrated images obtained from the recorded data of multiple time-lapse surveys (Hatchell 10 and Bourne 2005b; Røste et al. 2006; Hawkins et al. 2007). Such apparent displacements in 11 the subsurface, induced by relative velocity and strain changes, are measured by using cross-12 correlation of two data vintages (Rickett and Lumley 2001; Hall et al. 2005). However, cross-13 correlation methods provide poor resolution for apparent lateral (horizontal) displacements 14 because the cross-correlation function of two data sets generally has a very broad peak.

15 The apparent horizontal displacement is difficult to interpret because the resolution in seismic 16 images is more degraded in the horizontal than in the vertical (time or depth) directions by 17 the acquisition and processing methods employed (Hale 2009). Furthermore, in sedimentary 18 basins, the sedimentary structures are often close to horizontal layer section in seismic 19 images. Therefore, we tend to estimate mainly the vertical component of displacement, as it 20 is well resolved, but the lateral displacement components play an important role in better 21 aligning the seismic images and improving the estimates of difference in reflection amplitude 22 (Nickel et al. 2003) for time-lapse study. Therefore, all the displacement components must be 23 taken into account in order to estimate the changes in reservoir properties accurately. In order 24 to increase the vertical and lateral displacement resolution to sub-pixel scale, we propose a phase-correlation method developed in satellite imaging (Kuglin and Hines 1975;
 Puymbroeck *et al.* 2000).

3 Satellite images are being used to monitor natural phenomena such as earthquakes, 4 volcanoes, glacier flow and sand dune migration; processes that lead to topographical 5 changes (Puymbroeck et al. 2000; Binet and Bollinger 2005; Berthier et al. 2005; Crippen and Blom 1991). The earth surface changes can be determined by comparing two satellite 6 7 images acquired at different times. According to Leprince et al. (2008) it is necessary to 8 properly co-register the two images before measuring the deformation due to natural 9 phenomena (e.g. earthquakes). Similarly, in time-lapse seismic we acquire the seismic data 10 sets at different times to detect the changes at reservoir scale. Before the change detection in 11 the reservoir the two seismic images are properly matched or cross-equalized (Rickett and 12 Lumley 2001; Hatchell and Bourne, 2005a). Satellite images have the lateral resolutions of 13 5 m to 10 m, whereas deformations induced by earthquakes are often at centimetric, and 14 sometimes milimetric, scales, so it is essential to measure deformations at sub-pixel scales. 15 To measure the displacement at sub-pixel scale in satellite imaging, a phase-correlation 16 method has been proposed (Puymbroeck et al. 2000; Blaci et al. 2006; Leprince et al. 2008). 17 Even though seismic data have a spectral band different from that of satellite images, which may result in different correlation functions, the phase-correlation method can be used for 18 19 images with any spectral band (Leprince et al. 2008).

The most remarkable property of phase correlation over the standard cross-correlation is the resolution with which it can detect the correlation function peak. Figure 1 shows an example of two displaced areal images. Figures 1(a) and 1(b) are two satellite images acquired in Paris at two different times, where one of the images is slightly displaced. These satellite images have contrasts in both dimensions but are used here to illustrate the motivation of using

phase-correlation in satellite imaging. Figures 1(c) and 1(d) show the standard spatial crosscorrelation and the phase-correlation functions of these two images, respectively. The methods are described later in section 2. The phase-correlation provides a distinct and sharp peak while the cross-correlation yields several broad peaks. Note, that in this example, while the maximum of the main peak of the cross-correlation appears at the correction position but sometimes the maximum of the main peak might not be centered at the correct position (Foroosh *et al.* 2002), leading to inaccurate estimates of the lateral displacements.

8 The second important property of the phase-correlation is that it whitens the signal by 9 normalization, which makes the phase-correlation robust across different spectral bands 10 (Foroosh *et al.* 2002). These properties of the phase correlation lead to a sharp peak in all 11 directions (horizontal and vertical), providing better-resolved displacements in the horizontal 12 as well as vertical directions. Therefore, the phase-correlation method is routinely used for 13 satellite imaging.

14 Horizontal displacement in seismic images is measured by using various methods such as the non-rigid matching technique (Nickel and Sønneland 1999; Nickel et al. 2003) 3D matching 15 16 method (Aarre 2008), 7D warping (Hall 2006) and multidimensional warping by sequential 17 1D cross-correlation (Hale 2009). We have estimated the lateral displacement by using 18 phase-correlation here. Hale (2009) recognised the potential of the phase correlation method 19 but chose not to use this approach due to the fact that it can be computationally expensive. However, with modern computing technology, it is possible to exploit the strength of the 20 phase correlation method to obtain a better resolution shift measurement. This was 21 22 demonstrated in Tomar et al. (2014) where the sub-sample shifts are measured using phase 23 correlation method.

1 The sub-pixel scale in satellite imaging data corresponds to sub-sample scale measurements 2 in time-lapse seismic. Similar to satellite imaging, the displacement induced by relative 3 velocity changes in a reservoir due to production or injection of fluid could be much less than 4 a sampling interval, and therefore it becomes necessary to estimate the displacement 5 accurately at sub-sample scale. Such sub-sample measurement of displacements in the 6 subsurface serve two purposes. First, these displacements are used to align images, thereby 7 ensuring that all the events are co-located. Second, it is possible to obtain some important 8 information about changes inside and around the reservoir, such as fractional velocity change 9  $\partial v/v$ , and vertical strain  $\mathcal{E}_{zz}$ , as follows (Hatchell and Bourne 2005a):

10 
$$\frac{\partial v}{v} = -\frac{R+1}{R}\frac{d(\partial t)}{dt},$$
 (1)

11 
$$\varepsilon_{zz} = -\frac{1}{R} \frac{\partial v}{v},$$
 (2)

12 where *v* is the baseline P-wave velocity and  $\partial v$  is the change in the velocity between the 13 baseline and monitor data,  $\partial t$  is the time-shift and R is the dilation factor that is the relative 14 velocity change divided by the relative thickness change within a given layer (Hatchell and 15 Bourne 2005a, Røster *et al.* 2006, Carcione *et al.* 2007).

In this paper our objective is to estimate accurately the vertical and lateral displacement at sub-sample scale by taking advantage of the phase-correlation. After describing the theory of cross-correlation and phase correlation and presenting the data sets we show the synthetic as well as real data application of phase-correlation.

### 20 2. Methodology and data sets

#### 21 **2.1 Cross-correlation method**

1 The cross-correlation between two functions is a standard approach to feature detection as 2 well as to estimation of displacement components. Cross-correlation can be computed 3 efficiently in the time domain and the frequency domain. Let  $i_1$  and  $i_2$  be two images where 4 the second image is a version of the first image shifted by displacement ( $\Delta x$ ,  $\Delta y$ ) such that

5 
$$i_2(x,y) = i_1(x - \Delta x, y - \Delta y).$$
 (3)

6 In time-lapse seismic,  $i_1$  and  $i_2$  are the baseline and monitor images, respectively. If  $I_1$  and  $I_2$ 7 are the Fourier transforms (FT) of the images  $i_1$  and  $i_2$  then the cross-correlation in the space 8 domain would be the inverse Fourier transform (FT) of the cross-power spectrum. The cross-9 power spectrum is defined as the product of  $I_1$  and the complex conjugate of  $I_2$ . Based on the 10 convolution theorem of FT (Gonzalez and Woods 2002), cross-correlation is defined as:

11 
$$C(u,v) = F^{-1}\{I_1(\omega_x, \omega_y), I_2^*(\omega_x, \omega_y)\},$$
(4)

12 where \* represents the complex conjugate operator and  $F^{-1}$  is the inverse FT,  $\omega_x$  and  $\omega_y$  are 13 the frequency or wavenumber variables. If  $i_1$  and  $i_2$  are related by equation (3) then the shift 14 property of FT (Gonzalez and Woods 2002) states in the Fourier domain:

15 
$$I_2(\omega_x, \omega_y) = I_1(\omega_x, \omega_y)e^{-(\omega_x\Delta x + \omega_y\Delta y)}, \qquad (5)$$

16 where j = sqrt(-1) and therefore the cross-correlation becomes:

17 
$$C(u,v) = F^{-1} \{ M_1^2(\boldsymbol{\omega}_x, \boldsymbol{\omega}_y) e^{-j(\boldsymbol{\omega}_x \Delta x + \boldsymbol{\omega}_y \Delta y)} \},$$
(6)

18 where  $M_1^2 = I_1^* I_1$ .

Because the monitor image is considered as the shifted version of the base image therefore, it has been assumed as  $|I_1| = |I_2|$ . The above equations summarize the main principle of the frequency-domain, cross-correlation-based, translation estimation (Tzimiropoulos *et al.*) 1 2008). We then search for the maximum peak of the cross-correlation function locally to 2 estimate the shift between the two images  $i_1$  and  $i_2$  (Lewis 1995). It can be seen that phase 3 difference from the term  $exp\{-i(\omega_x\Delta x + \omega_v\Delta y)\}$  in equation (6), which contains the translation 4  $(\Delta x, \Delta y)$  is weighted by the squared magnitude  $M_1$ . We assume that the seismic image is 5 band-limited and is not aliased; therefore, due to the low pass nature of the image, the 6 weighting operation results in a peak of large magnitude in C, but the location of the peak 7 may be compromised if the weighting function has a peak at a location different from that of 8 the phase function. This problem can be tackled by using phase-correlation to measure the 9 translation between the images.

## 10 **2.2 Phase correlation method**

11 The phase correlation is derived from the Fourier shift theorem (Oppenheim *et al.* 1999), 12 where the relative displacement between a pair of similar images is retrieved from the phase 13 difference of their Fourier transforms. Let  $i_1$  and  $i_2$  be two images that differ only by a 14 displacement ( $\Delta x$ ,  $\Delta y$ ) as in equation (3). By using equation (5) obtained from the Fourier 15 shift theorem, the cross-power spectrum, that is the multiplication of the FT of the images  $i_1$ 16 and complex conjugate of the FT of image  $i_2$ , can be written as:

17 
$$C_{i_1,i_2}(\boldsymbol{\omega}_x,\boldsymbol{\omega}_y) = I_1(\boldsymbol{\omega}_x,\boldsymbol{\omega}_y)I_2^*(\boldsymbol{\omega}_x,\boldsymbol{\omega}_y), \qquad (7)$$

18 The normalized cross spectrum of the images  $i_1$  and  $i_2$  can be written as:

$$NC_{i_{1},i_{1}}(\boldsymbol{\omega}_{x},\boldsymbol{\omega}_{y}) = \frac{I_{1}(\boldsymbol{\omega}_{x},\boldsymbol{\omega}_{y})I_{2}^{*}(\boldsymbol{\omega}_{x},\boldsymbol{\omega}_{y})}{\left|I_{1}(\boldsymbol{\omega}_{x},\boldsymbol{\omega}_{y})I_{2}^{*}(\boldsymbol{\omega}_{x},\boldsymbol{\omega}_{y})\right|} = e^{-j(\boldsymbol{\omega}_{x}\Delta x + \boldsymbol{\omega}_{y}\Delta y)}$$
(8)

19

To stabilized the division to normalize the cross power spectrum we add an infinitesimal small value in the denominator, while computing the correlation function. The inverse 1 Fourier transform of the normalized cross-power spectrum is a band-limited, shifted delta 2 function centered at  $\Delta x$ ,  $\Delta y$ 

$$F^{-1}(e^{-j(\omega_x \Delta x + \omega_y \Delta y)}) = \delta(x + \Delta x, y + \Delta y).$$
<sup>(9)</sup>

4 It can be seen from equation (9) that we keep only the phase information because the 5 amplitude has been whitened by normalization. The relative displacement of these images 6 can then be estimated from the coordinates of the correlation peak. If the displacement 7 components are integer values then  $(\Delta x, \Delta y)$  can be measured by this method without any 8 further extension. But in case of sub-sample displacements ( $\Delta x(x,y)$  and  $\Delta y(x,y)$ ), the peak of 9 the correlation is not a Dirac delta function anymore, but a down-sampled version of a 10 Dirichlet kernel. An extension of phase correlation to sub-pixel registration has been used to 11 measure the displacement at sub-sample scale. To apply the phase correlation at sub-sample 12 scale the two images are considered as down sampled version of the original images and 13 approximated with the sinc function. For more detailed explanation about the extension of 14 phase correlation one can see (Foroosh et al. 2002). The identification of the main peak also 15 depends upon the signal to noise ratio of the images. But for the sub-sample shift the signal to 16 noise ratio is not of great concern, one can easily identify the main peak in sinc function. The 17 phase correlation method is applied iteratively to estimate the translations and these shifts are 18 applied to the monitor image to match it with the base image.

## 19 **2.3 Repeatability**

In order to estimate the sub-sample shifts, it is important that the data sets must be repeatable. The repeatability indicates the similarity between the base and monitor data sets after acquisition and processing. Repeatability could be measured by the normalized root-meansquare (*NRMS*) difference of two traces  $a_t$  and  $b_t$  within a given window  $t_1$ - $t_2$  (Kragh and Christie 2002), defined by the *RMS* difference of the traces divided by the average *RMS* of
 the two traces, expressed as:

3 
$$NRMS = \frac{200 \times RMS(a_t - b_t)}{RMS(a_t) + RMS(b_t)},$$
 (10)

4 where the *RMS* operator is defined as:

5 
$$RMS = \sqrt{\frac{\sum_{t_1}^{t_2} (x_t)^2}{N}},$$
 (11)

6 where, *N* is the number of samples present in the interval of  $t_1$ - $t_2$ . The values of *NRMS* are not 7 limited in the range of 0% to 100% but can reach to 200% (Kragh and Christie 2002). For 8 example, if the two traces are perfectly repeatable, the *NRMS* value will be zero and if the 9 two traces are anti correlated to each other, the *NRMS* value will be 200%, the theoretical 10 maximum.

#### 11 **2.4. Test Data Set**

12 In order to test the two methods discussed above, we take time-lapse data from the Norne oil 13 field. The Norne oil field is located in the Norwegian North Sea (Figure 2). The main field is 14 a 9 km x 3 km horst block composed of high-porosity, high-permeability, high net-to-gross 15 lower and middle Jurassic sandstones (Osdal and Alsos 2002, Aarre 2008). The field was 16 discovered in 1991 and it started producing oil in 1997. The base data set was acquired in 17 2001 and monitor data sets were acquired in 2003, 2004 and 2006 by using steerable 18 streamers and a highly repeatable acquisition system. These data sets were processed in an 19 identical manner using conventional steps followed by a Kirchhoff prestack time migration 20 (Yilmaz 2001) to image time-lapse seismic changes. Osdal et al. (2006) and Aarre (2008) 21 provide detailed descriptions of the field geology, its production history, seismic data

acquisition and processing and some preliminary interpretation of the observed time-lapse
 seismic amplitudes.

To test the feasibility of the phase correlation method we first apply both the crosscorrelation and phase correlation methods to a part of the Norne data. Figure 3 shows an example of two seismic images baseline 2001 (a) and monitor 2006 (b) from Norne oil field, the standard cross-correlation (c) and the phase-correlation (d) of data within the white rectangular window indicated in the seismic images and the zoomed panels are shown in Figures 3(a1) and 3(b1). From Figures 3(c) and 3(d) it can be seen that phase-correlation provides a single distinct and sharp peak while cross-correlation yields several broad peaks.

## 10 3 Synthetic data and shift measurements

## 11 **3.1 Synthetic Data Example**

12 A synthetic data set was created using the Norne data, 301 traces and 301 time samples  $(i_1)$ 13 (Figure 4a) were taken from the 2001 survey. In the Norne data set the vertical sampling 14 interval is 4 ms and horizontal sampling interval is 12.5 m. We applied an elliptical vertical 15 time shift of  $\Delta x$  (Figure 4c) and two positive and negative lobes in the horizontal 16 displacement of  $\pm \Delta y$  (Figure 4d) providing the time-lapse monitor image (*i*<sub>2</sub>) (Figure 4b). In 17 the paper we have used  $\Delta x$  for the time shift instead of  $\Delta t$  for the explanation, therefore, it 18 does not change the unit of time and x can be correspond to the vertical time in whole text. 19 The time-lapse image  $(i_2)$  is related to the base image as follow:

20 
$$i_2 = i_1(x + \Delta x(x, y), y + \Delta y(x, y))$$

(12)

21

These displacement components represent the vertical downward and the horizontal outward displacement of image point in  $i_1$  relative to the image  $i_2$ . The only difference between these

1 two images is the misalignment of the image point described in the displacement images 2  $\Delta x(x,y)$  and  $\Delta y(x,y)$ . For the synthetic images, the assumption is made that the noise level of 3 the two images is same. Our aim is to measure sub-sample shifts between these two seismic 4 images, so vertical and horizontal displacement components have been taken to be a 5 maximum of one sample shift in each direction. The minimum time shift is equal to 0.08 ms 6 i.e. 2% of the vertical sampling interval, and the minimum horizontal displacement is equal to 7 the  $\pm 0.25$  m, also 2% of the horizontal sampling interval. These shifts vary linearly from the 8 maximum of one sample in each direction, i.e. 4 ms in vertical direction and 12.5 m in 9 horizontal direction, to minimum in the form of an ellipse for the time shift and two positive 10 and negative blobs for the distance (Figures 4c and 4d). The shift magnitude in each direction 11 is purely for evaluating shift detection resolution. The shift necessary for accurate estimation 12 of reflection amplitude changes at the reservoir is outside the scope of this paper.

Since the shifts are not integer multiples of the sampling, it is necessary to interpolate the image  $i_1$  to construct the image  $i_2$  with the synthetic displacement components in both directions. A cubic spline interpolation method (Press *et al.* 1996) has been used to apply the vertical  $\Delta x(x,y)$  and horizontal  $\Delta y(x,y)$  displacement components to the image  $i_1$  for constructing time-lapse image  $i_2$ . After applying the shift, we re-interpolate the image  $i_2$  to its original sampling intervals, which are the 4 ms in the vertical direction and 12.5 m in horizontal direction by using the same cubic spline interpolation method.

After creating the time-lapse image, we use these two images  $(i_1 \text{ and } i_2)$  to recover the vertical  $(\Delta x)$  and horizontal displacement  $(\Delta y)$  components, using the cross-correlation and the phase-correlation methods. For estimating displacement vectors we search for the locations of the maxima of the peak of cross-correlation and phase-correlation locally by using a sliding Gaussian window *w*:

$$w(k_x,k_y) = e^{-(\frac{k_x^2}{2\sigma_x^2} + \frac{k_y^2}{2\sigma_y^2})},$$
(13)

2 where  $\sigma_x$  and  $\sigma_y$  are the standard deviation of the Gaussian window in the horizontal and 3 vertical directions respectively,  $k_x$  is the distance from the centre in the horizontal axis and  $k_y$ 4 is the distance from the centre in the vertical axis. Different values of  $\sigma_x$  and  $\sigma_y$  would result 5 in an elliptical window function instead of the circular window used here. The effect of the small and large radius has been shown in appendix A1: if the window radius is too small or 6 too large then the shift measurement could be biased. The choice of the variance of the 7 8 Gaussian is extremely application dependent but should be small enough to measure the shift 9 locally. Therefore, we can say that standard deviation of 5 samples is a good compromise for 10 the data set we have used in this paper. The Gaussian kernel has been chosen on the basis of the relation between the kernel size and standard deviation (kernel size =  $6\sigma$  -1), the 11 explanation for which is given in appendix A1. Here, we have used  $\sigma = 5$  samples and kernel 12 size = 6\*5 - 1 = 29 samples i.e. 116 ms two-way travel time and 362.5 m along the horizontal 13 14 axis for correlation with the radius of  $3\sigma$ . The Gaussian window is applied to the image 15 sample that is chosen from both base and monitor images.

#### 16 **3.2 Shift measurement by cross-correlation**

1

Figures 5(a) and 5(b) show the estimation of the displacement vector components by using local standard cross-correlation between the seismic images in Figures 4(a) and 4(b). The Gaussian window w makes the cross-correlation function local and enables the local estimate of the displacements. From Figure 5(a) we can see that the vertical displacement map is consistent with the actual synthetic time shift in Figure 4(c) applied to the base image while the horizontal displacement in Figure 5(b) is not well resolved. The difference maps of Figures 4(a) and 4(b) are shown before (Figure 5c) and after (Figure 5e) application of the

1 shifts estimated from cross-correlation. Figure 5(e) clearly shows that the residual amplitude 2 difference between the base and corrected monitor images decreases but that there is still 3 significant difference in the images because the horizontal displacement map is not well 4 resolved by the cross-correlation. The measured vertical and horizontal displacement 5 components  $(\Delta x, \Delta y)$  between the images  $i_1$  and  $i_2$  are applied to the monitor image  $i_2$ , to align 6 the time-lapse image vertically and horizontally with the base image  $i_1$  using a cubic spline 7 interpolation method. NRMS maps were also computed using equation (10) before (Figure 8 5d) and after (Figure 5f) alignment of the images, here the maximum value of NRMS reaches 9 to 121.6% because the displacement maps have higher values in the center and lower values 10 towards the edges. NRMS between the two images is computed trace by trace by using a 11 vertically sliding window of 29 time-samples. The root mean square error (RMSE) is also 12 computed using

13 
$$RMSE = \sqrt{\frac{1}{N} \sum_{i=1}^{N} (A_i - M_i)^2}$$
(14)

14 where, *RMSE* is root mean square error,  $A_i$  is actual shift and  $M_i$  is measured shift at  $i^{th}$ 15 sample point and N is the number of samples in one trace. RMSE is measured trace by trace 16 between the actual and measured synthetic time-shift and horizontal displacement. Figures 17 5(g) and 5(h) show the RMSE estimated in percentage for the time-shift and horizontal 18 displacement maps respectively. It can be seen that the maximum RMSE in time-shift 19 measurement is less than 5% but for the horizontal displacement it is 22%. This might be the 20 reason for the broader peak in the horizontal direction in the correlation function. Since, the 21 displacement varies in both directions, vertically and laterally, high amplitude events might 22 slide in and out of the local Gaussian window, leading to several peaks, and hence non-23 uniqueness of the solution (Hale 2009).

#### 1 **3.3 Shift measurement by phase-correlation**

2 Figure 6 shows the estimation of the displacement vector using the local phase-correlation 3 method. The same sliding Gaussian window is used as for the cross-correlation in the 4 previous section. We use several steps using phase correlation as follows: in step 1, we select 5 the local Gaussian window from the two images, in step 2 we compute cross power spectrum 6 of these two image samples, in step 3 we normalize the cross-power spectrum, in step 4 we 7 apply the inverse Fourier transform to get the shift delta function and in step 5 we look for 8 the maximum peak to get the displacements in both directions. These steps are repeated for 9 each image sample. Because the phase-correlation peak is well resolved in both directions, 10 the vertical (Figure 6a) and horizontal (Figure 6b) components of displacement are consistent 11 with the actual synthetic shifts in Figures 4(c) and 4(d) applied to the base image. We have 12 smoothed the correlation coefficient by averaging the values from the neighboring traces.

13 The initial difference and NRMS maps between the two seismic images  $i_1$  and  $i_2$  are shown in 14 the Figure 5(c) and 5(d), respectively. Figures 7(a) and 7(b) show the difference and NRMS 15 maps between the base and monitor images after vertical matching. There is a large residual 16 difference after aligning the images vertically indicating poor alignment: the maximum value 17 of the NRMS reduces to 59 % because horizontal alignment has not yet been applied. Figures 18 7(c) and 7(d) show the difference and *NRMS* maps between the two seismic images after the 19 alignment vertically and horizontally. The difference and NRMS values improve 20 significantly, the maximum of the NRMS reduces to 21.2% after horizontal alignment of the images. On the basis of the NRMS values, we could say that the residual amplitude 21 22 differences between the base image and aligned images are negligible compared to the initial 23 difference, the difference decreases by a factor of 6.67, estimated by taking the ratio between 24 the absolute maximum amplitude of the initial difference (Figure 5c) and the absolute

1 maximum amplitude of the difference after alignment (Figure 7c). The RMSE is measured 2 trace by trace between the actual and measured synthetic time-shift and horizontal 3 displacement using equation (14). Figures 7(e) and 7(f) show RMSE in percentage of the 4 time-shift and horizontal displacement maps, respectively. It can be seen that the maximum 5 RMSE time-shift is less than 5%, while in horizontal displacement RMSE is around 8%, a 6 significant improvement over the *RMSE* for the cross-correlation in Figures 5(g) and 5(h). 7 From the above observations it can be seen that the displacement maps estimated by phase-8 correlation have better accuracy than those estimated by cross-correlation. RMSE in 9 horizontal displacement is improved more than in vertical displacement, suggesting that 10 phase correlation plays an important role in matching images in both horizontal and vertical 11 directions.

## 12 **3.3.1** Cyclic search of the shift using phase-correlation

13 After comparing phase-correlation and cross-correlation, the time-shift and horizontal 14 component displacements were measured iteratively using phase-correlation; this cyclic 15 search was introduced by Hale (2009). First we compute the vertical and horizontal 16 displacement components ( $\Delta x$ ,  $\Delta y$ ) between the images  $i_1$  and  $i_2$  using phase-correlation, then 17 we apply these displacement components to the monitor image  $i_2$ , to align the time-lapse 18 image vertically and horizontally with the base image  $i_1$ . Since the displacement components 19 are not integers, we used a cubic spline interpolation to apply the vertical and horizontal 20 shifts to the monitor image  $i_2$ . After estimating and applying these displacement components 21 for each image axis, we repeated this procedure to align the monitor image to base image 22 until the vertical and horizontal displacement components were negligible and these 23 measured shifts were summed. We computed NRMS between the base and monitor images 24 using equation (10) to measure the differences between the two images after the alignment.

1 Figure 8 shows the estimated displacement images by using the iterated phase-correlation 2 method. Figures 8(a) and 8(b) show the estimated time shift and horizontal displacement after 3 the second iteration. Because the shift measurements converge towards the actual shift just 4 after two iterations therefore, it could be called as the two steps approach. From these 5 displacement images, it can be seen that the time shift and horizontal displacement converge 6 towards the actual displacements in Figures 4(c) and 4(d), respectively, after two iterations. 7 Figures 8(c) and 8(d) show the difference and NRMS maps between the base image and 8 aligned image after two iterations. However, using phase-correlation and applying the 9 displacements iteratively to the monitor image, the residual amplitude differences between 10 the base image and aligned images are reduced further compared to the initial difference; the 11 difference is decreased by a factor of 8 between the images 5(c) and 8(c). There are still small 12 residual amplitude differences remaining between the images because of the limitation of the 13 interpolation method. After a significant level of alignment, we are not able to produce 14 perfect alignment. As stated before the estimated displacements serve two general purposes: 15 firstly, enabling more accurate amplitude difference estimates between the baseline and 16 aligned monitor images, and secondly, it is possible to obtain important information about 17 changes within and around the reservoir from these apparent displacements.

## 18 **3.3.2 Shift measurement after adding white noise**

We added white noise to the base image  $i_1$  with a signal-to-noise ratio of 25 dB and computed the vertical and horizontal shifts between that image and the monitor image  $i_2$  by using phasecorrelation. The noise is added only in the base image because we want to consider the different noise level in both of the images. In this example the noise levels of the two images are different, as the white noise is added only to the base image. Figure 9(a) shows the white noise added to the base image; Figure 9(b) shows the difference between the base image with 1 noise and the monitor image. Now the time-lapse changes in the difference image are induced 2 not only by the synthetic shift but also due to noise; therefore, residual amplitude differences 3 between the base and monitor images are present throughout the image. After adding the 4 noise, the maximum NRMS value also change from initial 121.6 % to 128.7%. The time-shift 5 and horizontal displacement maps are computed and shown in Figures 9(c) and 9(d), 6 respectively. The shifts estimated after adding the noise are consistent with the actual 7 synthetic shift. The shifts are measured using cross-correlation after adding the white noise in 8 appendix A2.

## 9 4. Application to Real Data

We applied the phase-correlation method to real data from the Norne oil field (Figure 2). As mentioned before, the base data set was acquired in 2001 and monitor data sets were acquired in 2003, 2004 and 2006. Here we use the 2001 base data and 2006 monitor data. Figure 10 presents 2D full stack images from baseline (Figure 10a) and monitor (Figure 10b) survey, and the difference between the two vintages is shown in Figure 10(c).

15 The vertical time shift (Figure 11a) and horizontal shift (Figure 11b) have been measured 16 between baseline and monitor images using the phase-correlation method. For the real data 17 set we use the same Gaussian window as was used for the synthetic data set. We get 18 maximum negative time shift of 1.25 samples i.e. 1.25x4 = 5 ms (slightly more than time 19 sampling interval of 4 ms), and maximum horizontal displacement of 0.74 samples i.e. 20  $2.5 \times 0.74 = 9.2$  m (less than the horizontal sampling interval of 12.5 m). We find a negative 21 time shift below the reservoir that is the pull-up effect due to an increase in velocity in the 22 reservoir following the production. Such shifts have been observed in the Norne oil field by Aarre (2008) using 3D matching method. In the time shift image (Figure 11a) we observe a 23 24 gap in the negative time shift around 3.1 s because the image contains an inter-bed multiple

from a shallower layer at that time; the multiple is not affected by the pull-up induced by
 velocity change in reservoir (Aarre private communication). That particular multiple is a peg leg/ghost of the top-reservoir interface.

4 We should find a constant time shift throughout the region below the reservoir if the time 5 shift were due to the pull-up effect and the ray-paths were vertical. However, we do not find a 6 laterally invariant time shift below 3.6 s. This is because, just below the reservoir, all the 7 down- and up-going rays in a common mid-point gather pass through the altered reservoir, 8 while far below the reservoir few down- and up-going rays go through the altered reservoir. 9 This is the under-shooting effect. Furthermore, noise usually increases with depth in the 10 image. In Norne oil field, the data are noisier below 3.6 s, as can be seen from the difference 11 between the base and monitor vintages, since the noise is not affected by velocity-induced 12 time shifts in the reservoir. We find horizontal shifts in the subsurface; many possible causes 13 of this apparent horizontal shift have been discussed in Aarre (2008). An analysis of the 14 estimated displacements suggests around 5% of velocity change in the reservoir between the 2001 and 2006 by using equation (1). We have assumed a constant dilation factor R = 5 in 15 16 equation (1), which is within the range of the dilation factor observed for the North Sea 17 (Hatchell and Bourne, 2005a).

#### 18 **5. Discussion and future work**

A phase-correlation method has been described in this paper for measuring the sub-sample time-shift and displacement components in time-lapse seismic. By analyzing the observed time-shifts in the real data we estimate that between 2001 and 2006 a 5% velocity change occurred during the production period by assuming a dilation factor of R = 5 (Hatchell and Bourne, 2005a). However, the true value could well be different from 5.

1 We have also made some assumption that the images are cross-equalized properly and have 2 the same level of the noise before measuring the displacement maps in a synthetic data 3 example. In the presence of noise and dissimilar parts of the images, the value of the phase-4 correlation peak might be significantly reduced and the method may become unstable. From 5 the example of the showed in the 3.3.2 the synthetic data with white noise, it can be seen that 6 the shift measurement is continuous with the actual shift while the different amount of the 7 noise has not been tested and the actual seismic noise is not added in the data set, which need 8 to be further investigated. In the Norne oil field, we know that the data sets are acquired with 9 the same instrument but if the data sets are acquired by different instrument then the 10 measurement of the displacements  $(\Delta x, \Delta y)$  might be biased. In this paper a circular window 11 with a specific radius value have been chosen; the window could be circular or elliptical and 12 its dimensions must bigger than the wavelength of the anomaly. Displacement components as 13 small as 2% of the sampling interval have been estimated. However; a complete analysis of 14 the sensitivity of reservoir amplitude changes to the amount of image displacement is out of 15 the scope of this paper.

#### 16 **6.** Conclusion

17 Phase-correlation is a technique developed in satellite imaging for sub-pixel image co-18 registration. We have proposed phase-correlation in time-lapse seismic and applied it to 19 synthetic and real data sets for estimating sub-sample vertical (time-shift) and horizontal displacement components. It is possible to obtain high-resolution vertical and horizontal 20 21 displacement components between the baseline and monitor data sets by using phase-22 correlation. These displacement components contain important information about the changes 23 within and around the reservoir. Vertical and horizontal components of displacement as small 24 as 2% of the sampling interval have been estimated for a synthetic data set. Phase-correlation 1 can measure the shift to a significantly low scale. However, the significance of any 2 estimation after a certain number of resolution is obviously limited by the signal to noise ratio 3 in time-lapse seismic. To register the two images properly all the displacement components 4 have to be taken into account. We have applied this method to a real data set from the Norne 5 oil field and have obtained vertical (time shift) and horizontal displacement maps. Using 6 phase-correlation method both the vertical and horizontal shifts can be estimated precisely at 7 sub-sample scale. We have estimated 5% velocity change in the Norne oil field during 8 production between 2001 and 2006 data sets on the basis of the time-shift computed by using 9 phase-correlation method.

## 10 Acknowledgement

We gratefully acknowledge the support of Schlumberger and Total in this project and their permission to publish this paper. However, the views expressed here are those of the authors who are solely responsible for any errors. We give our sincere thanks to Statoil and partners for releasing the Norne data through the NTNU/IO CENTRE. We are also thankful to Victor Aarre for providing the interpretation information of the real data and fruitful discussion. We give our sincere thanks to Phil Christie and Aline Gendrin-Brokmannat Schlumberger for the suggestions to improve and review the paper.

18

19

20

21

#### 22 **References**

1	• Aarre V. 2008. On the presence, and possible causes, of apparent lateral shifts below the
2	Nome reservoir. SEG Technical Program Expanded Abstracts, 27, 3174–3178.
3	• Balci M. and Foroosh H. 2006. Subpixel estimation of shifts directly in the Fourier
4	domain. IEEE Transactions on Image Processing, 15, 1965–1972.
5	• Berthier E., Vadon H., Baratoux D., Arnaud Y., Vincent C., Feigl K., Remy F. and Legresy
6	B. 2005. Surface motion of mountain glaciers derived from satellite optical
7	imagery. Remote Sensing Environment, 95, 14–28.
8	• Binet R. and Bollinger L. 2005. Horizontal coseismic deformation of the 2003 Bam (Iran)
9	earthquake measured from SPOT-5 THR satellite imagery. Geophysical Research
10	Letter, 32, (2), L02307.1–L02307.4.
11	• Crippen R. and Blom R. 1991. Measurement of subresolution terrain displacements using
12	SPOT panchromatic imagery. in Proc. IGARSS, 3, 1667–1670.
13	• Carcione J. M., Landrø M., Gangi A. and Cavallini, F. 2007. Determining the dilation
14	factor in 4D monitoring of compacting reservoirs by rock-physics
15	models. Geophysical Prospecting, 55, (6), 793-804
16	• Dong-Min W., Dong-Chul P., Ilhwan C., Taikyeong J. and Yunsik L. 2010. Effects of the
17	change of window size on the performance of correlation-based stereo.
18	Information Networking and Automation (ICINA), International Conference, 2,
19	364-368.
20	• Gonzalez R.C. and Woods R.E. 2002. Digital Image Processing, 2nd edition. Pearson
21	Education, Singapore, ISBN 0-201-18075-8.

1	• Foroosh H., Zerubia, JB. and Berthod M. 2002. Extension of phase-correlation to subpixel
2	registration. IEEE Transactions on Image Processing, 11, 1057Transa
3	• Hale D. 2009. A method for estimating apparent displacement vectors from time-lapse
4	seismic images. Geophysics, 74, (5), V99–V107.
5	• Hall S. A., MacBeth C., Barkved O. I. and Wild P. 2005. Cross-matching with interpreted
6	warping of 3d streamer and 3d ocean-bottom-cable data at Valhall for time-lapse
7	assessment. Geophysical Prospecting, 53, 283–297.
8	• Hall S. 2006. A methodology for 7D warping and deformation monitoring using time-
9	lapse seismic data. Geophysics, 71, (4), O21–O31.
10	• Hatchell P. and Bourne S. 2005a. Rocks under strain: Strain-induced time-lapse time shifts
11	are observed for depleting reservoirs. The Leading Edge, 24, 1222–1225.
12	• Hatchell P. and Bourne S. 2005b. Measuring reservoir compaction using time-lapse time
13	shifts. 75th Annual International Meeting, SEG, Expanded Abstracts, 2500–2504.
14	• Hawkins K., Howe S., Hollingworth S., Conroy G., Ben-Brahim L., Tindle C., Taylor N.,
15	Joffroy G. and Onaisi A. 2007. Production-induced stresses from time-lapse time
16	shifts: A geomechanics case study from Franklin and Elgin fields. The Leading
17	Edge, 26, 655–662.
18	• Johnston D. H. 2013. Practical applications of time-lapse seismic data. Distinguished
19	Instructor Series, Society of Exploration Geophysicists.
20	• Kragh E. and Christie P. 2002. Seismic repeatability, normalized rms and predictability.
21	The Leading Edge, 21, 640–647.

1	• Kuglin C. D. and Hines D. C. 1975. The phase correlation image alignment method. IEEE
2	Proceedings of the International Conference on Cybernetics and Society, 163–165.
3	• Landro, M., Solheim O. A., Hilde E., Ekren B. O. and Stronen L. K. 1999. The Gullfaks
4	4d seismic study. Petroleum Geoscience, 5, 213–226.
5	• Leprince S., Barbot S., Ayoub F. and Avouac J. P. 2008. Automatic and precise ortho-
6	rectification, coregistration, and subpixel correlation of satellite images,
7	application to ground deformation measurements. IEEE Transactions on
8	Geoscience and Remote Sensing, 45, (6), 1529-1558.
9	• Lewis J. P. 1995. Fast Template Matching. Vision Interface, 95, (120123), 15-19.
10	• McPherson and Glen 2013. Statistics in scientific investigation : Its basis, application and
11	interpretation. Springer-Verlag. ISBN 9781475742909.
12	• Nickel M. and Sønneland, L. 1999. Nonrigid matching of migrated time-lapse seismic.
13	69th Annual International Meeting, SEG, Expanded Abstracts, 872-875.
14	• Nickel M., Schlaf J. and Sønneland L. 2003. New tools for 4D seismic analysis in
15	compacting reservoirs. Petroleum Geoscience, 9, 53-59.
16	• Oppenheim A., Schafer R. and Buck J. 1999. Discrete-time signal processing, 2nd editon.
17	Upper Saddle River, NJ Prentice-Hall, ISBN 0-137-54920-2.
18	• Osdal B., and Alsos T. 2002. Seismic modelling of eclipse simulations and comparison
19	with real 4D data at the Norne field. 64th Annual Conference and Exhibition,
20	EAGE, Extended Abstracts, A29.

1	• Osdal, B., Husby O., Aronsen H. A., Chen N. and Alsos T., 2006. Mapping the fluid front
2	and pressure buildup using 4D data on Norne field. The Leading Edge, 25, 1134-
3	1141.
4	• Press W. H., Teukolsky S. A., Vetterling W. T. and Flannery B. P. 1996. Numerical
5	recipes in fortran 90: The art of parallel scientific computing. Cambridge
6	University Press. FORTRAN Numerical Recipes.
7	• Puymbroeck N. V., Michel R., Binet R., Avouac J. P. and Taboury J. 2000. Measuring
8	earthquakes from optical satellite images. Applied Optics, 39, 3486-3494.
9	• Rickett J. E. and Lumley D. E. 2001. Cross-equalization data processing for time-lapse
10	seismic reservoir monitoring: A case study from the Gulf of Mexico. Geophysics,
11	66, (4), 1015–1025.
12	• Røster T., Stovas A. and Landrø M. 2006. Estimation of layer thickness and velocity
13	changes using 4d prestack seismic data. Geophysics, 71, (6), S219–S234.
14	• Tomar G., Singh S. and Montagner G.P. 2015. Sub-sample time shift and displacement
15	measurement by phase-correlation in time-lapse seismic. 76th EAGE conference
16	and exhibition Amsterdam, Extended abstract WE P06-03.
17	• Tzimiropoulos G., Argyriou V. and Stathaki T. 2008. A Frequency Domain Approach to
18	Roto-translation Estimation using Gradient Cross-Correlation. IEEE, in Proc.
19	BMVC.
20	• Yilmaz, Öz 2001. Seismic data analysis. Society of Exploration Geophysicists, ISBN 1-
21	56080-094-1.

- 1
- 2
- 3

# 4 Appendix A1

5 To measure the displacement map locally in the synthetic and real data examples we have 6 used Gaussian window *w*:

7 
$$w(k_x, k_y) = e^{-(\frac{k_x^2}{2\sigma_x^2} + \frac{k_y^2}{2\sigma_y^2})}$$
(A1)

8 where  $\sigma_x$  and  $\sigma_y$  are the standard deviation of the Gaussian window in horizontal and vertical 9 direction respectively,  $k_x$  is the distance from the centre in the horizontal axis and  $k_y$  is the 10 distance from the centre in the vertical axis.  $k_x$  and  $k_x$  are in the range  $(-3\sigma_x)$  to  $(3\sigma_y)$  from the 11 centre as a rule of thumb on the basis of the normal distribution (McPherson and Glen, 2013) 12 to comprise more than the 99% region of the Gaussian integral. Therefore, the optimum 13 Gaussian kernel size would be  $(3\sigma + 3\sigma - 1 = 6\sigma - 1)$  samples with the radius of  $3\sigma$ . Here, 14 some examples have been shown with the different radius and kennel size of the Gaussian 15 window. We have taken the window size of 29 samples, which is an optimum window size as 16 a large window of the kernel size is not effective to get local shift. On the other hand a small 17 window is not very effective either, because a small window exhibits an undesirable effect 18 due to high noise level in the data (Dong-min et al. 2010). 29 samples of window size 19 correspond to 29x4 = 116 ms and 29x12.5 = 362.5 m in the vertical and horizontal directions 20 respectively.

We have obtained the above values of  $k_x$  and  $k_y$  and  $\sigma_x$  and  $\sigma_y$  after extensive testing. We demonstrate the effect of different values of kernel size and radius using three examples. 1 Figure A1(a) shows a Gaussian window for a radius ( $\sigma_x = \sigma_y$ ) of 2 and a kernel ( $k_x = k_y$ ) of 29 samples. We used this Gaussian window to estimate vertical (time) shift (Figure A1b) and 2 3 horizontal displacement (Figure A1c) maps using local phase correlation. In the second test, 4 the radius was increased to 5 samples, keeping the kernel fixed to 29. Figure A2(a) shows the 5 Gaussian whereas the corresponding vertical (time) shift and (c) horizontal displacement map 6 as shown in Figures A2(b) and A2(c). In the third test the radius was increased to 8. Figure 7 A3(a) shows the Gaussian window. The corresponding estimated vertical (time) shift and 8 horizontal displacement maps are shown in Figures A3(b) and A3(c).

9 From these examples, we can see that when the radius is small we use fewer of the data and 10 the results are biased, whereas for a radius of 5, the results are consistent with the actual 11 displacement map. When we use a higher radius of 8, then we get ringing results. Therefore, 12 if we take smaller and bigger radii then we do not get a good result. The choice of the 13 variance of the Gaussian is extremely application dependent. So we can say that radius of 5 is 14 a good compromise for the data set we have used in this paper with the 29 samples of kernel 15 size. Therefore, we have used the window size of 29 samples i.e. 116 ms two-way travel time 16 and 362.5 m along horizontal axis for correlation with the radius in vertical direction is 20 ms 17 and in horizontal direction is 62.5 m for synthetic as well as real data sets.

## 18 Appendix A2

The time shift and horizontal displacement are measured using classical crosscorrelation between the base image with white noise and the monitor image used in section 3.2.2. The effect of the noise does not really affect the shift measurement like phase-correlation. The shift measurement with noise vertical (time) shift (Figure A4a) and horizontal displacement (Figure A4b) are similar to the shift measured in Figure 5(a) and 5(b).